Accepted Manuscript

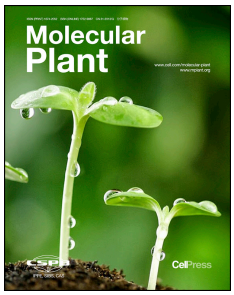

The role of UDP-glucuronic acid decarboxylase (UXS) in xylan biosynthesis in *Arabidopsis*

Beiqing Kuang, Xianhai Zhao, Chun Zhou, Wei Zeng, Junli Ren, Berit Ebert, Cherie T. Beahan, Xiaomei Deng, Qingyin Zeng, Gongke Zhou, Monika S. Doblin, Joshua L. Heazlewood, Antony Bacic, Xiaoyang Chen, Ai-Min Wu

PII: S1674-2052(16)30050-8
DOI: 10.1016/j.molp.2016.04.013
Reference: MOLP 289

To appear in: *MOLECULAR PLANT*
Accepted Date: 26 April 2016

Please cite this article as: **Kuang B., Zhao X., Zhou C., Zeng W., Ren J., Ebert B., Beahan C.T, Deng X., Zeng Q., Zhou G., Doblin M.S, Heazlewood J.L., Bacic A., Chen X., and Wu A.-M.** (2016). The role of UDP-glucuronic acid decarboxylase (UXS) in xylan biosynthesis in *Arabidopsis*. Mol. Plant. doi: 10.1016/j.molp.2016.04.013.

The role of UDP-glucuronic acid decarboxylase (UXS) in xylan biosynthesis in *Arabidopsis*

Beiqing Kuang[1,2+], Xianhai Zhao[1,2+], Chun Zhou[1,2], Wei Zeng[3], Junli Ren[4], Berit Ebert[3], Cherie T Beahan[3], Xiaomei Deng[2], Qingyin Zeng[5], Gongke Zhou[6], Monika S Doblin[3], Joshua L. Heazlewood[3,7], Antony Bacic[3], Xiaoyang Chen[1,2 *], Ai-Min Wu[1,2 *]

[1] State Key Laboratory for Conservation and Utilization of Subtropical Agro-bioresources, South China Agricultural University, Guangzhou, 510642, China;

[2] Guangdong Key Laboratory for Innovative Development and Utilization of Forest Plant Germplasm, College of Forest, South China Agricultural University. Guangzhou, 510642, China;

[3] ARC Centre of Excellence in Plant Cell Walls, School of BioSciences, The University of Melbourne, Parkville VIC 3010, Australia;

[4] State Key Laboratory of Pulp and Paper Engineering, South China University of Technology, Guangzhou, 510640, China;

[5] Institute of Botany, The Chinese Academy of Science, Beijing, 100093, China;

[6] Qingdao Institute of Bioenergy and Bioprocess Technology, Chinese Academy of Sciences, Qingdao, 266101, China;

[7] Joint BioEnergy Institute and Physical Biosciences Division, Lawrence Berkeley National Laboratory, Berkeley, California, 94720, USA;

* Corresponding authors: Xiaoyang Chen (xychen@scau.edu.cn) and Ai-Min Wu (wuaimin@scau.edu.cn)

+ These authors contributed equally to this work.

Running head: Cytosolic AtUXS can affect xylan synthesis

Abstract

UDP-xylose (UDP-Xyl) is the Xyl donor used in the synthesis of major plant cell wall polysaccharides such as xylan (as a backbone-chain monosaccharide) and xyloglucan (as a branching monosaccharide). The biosynthesis of UDP-Xyl from UDP-glucuronic acid (UDP-GlcA) is irreversibly catalyzed by UDP-glucuronic acid decarboxylase (UXS). Until now, little is known about the physiological roles of AtUXS in plants. Here, we report that *AtUXS1*, *AtUXS2* and *AtUXS4* are located in the Golgi apparatus whereas *AtUXS3*, *AtUXS5* and *AtUXS6* are located in the cytosol. Although all six single *AtUXS* T-DNA mutants and the *uxs1usx2uxs4* triple mutant show no obvious phenotype, the *uxs3uxs5uxs6* triple mutant has an irregular xylem phenotype. Monosaccharide analysis showed that Xyl levels decreased in the *uxs3uxs5uxs6* mutant and linkage analysis confirmed that the content of xylan in the *uxs3xus5uxs6* mutant declined, indicating that UDP-Xyl from cytosol AtUXS participates in xylan synthesis. Gel permeation chromatography (GPC) shows that the molecular weight of non-cellulosic polysaccharides in the triple mutants, mainly composed of xylans, is lower than in wild type, suggesting an effect on the elongation of the xylan backbone. For saccharification treatment, stems of the *uxs3uxs5uxs6* triple mutants released monosaccharides at a higher efficiency than those of wild type. Our results show that the cytosol UXS play a more important role than the Golgi localized UXS in xylan biosynthesis.

INTRODUCTION

Plant cell wall polysaccharides consist of cellulose and non-cellulosic polysaccharides and are a major source of renewable biomass. They play important roles in cellular growth and differentiation, and plant morphology and architecture, as well as provide an energy reserve (Doblin et al., 2010; Pauly and Keegstra, 2010). Generally, plants utilize sunlight to convert H_2O and CO_2 into sugars in the chloroplast. These sugars pass through a series of enzyme-catalyzed pathways, including nucleotide sugar metabolism, and accumulate as starch and sucrose in fruits and tubers as well as in cell wall polysaccharides and glycoproteins (Okazawa et al., 1993; Reiter and Vanzin, 2001; Seifert, 2004). The activated sugar donors of cell wall polysaccharides are nucleoside diphosphate (NDP) sugars, including UDP-D-glucose (UDP-Glc), UDP-D-glucuronate (UDP-GlcA), UDP-D-xylose (UDP-Xyl), UDP-D-galactose (UDP-Gal), UDP-D-galacturonate (UDP-GalA), UDP-D-apiose (UDP-Api), UDP-L-arabinose (UDP-Ara) UDP-L-rhamnose (UDP-Rha) and GDP-D-mannose (GDP-Man) (Reiter, 2008).

UDP-Xyl is an essential glycosyl donor required for the biosynthesis of heteroxylans and xyloglucans (Hayashi et al., 1988; Ray, 1980; Reiter, 2008; Rodgers and Bolwell, 1992) and for the side-chains of two types of pectin, xylogalacturonan and rhamnogalacturonan II (RGII). In addition, UDP-Xyl is the donor for glycoprotein, proteoglycan and glycolipid synthesis (Gotting et al., 2000; Seifert, 2004; Strasser et al., 2000). Mutant analyses suggest that *IRX9*, *IRX10* and *IRX14* and their homologs encode enzymes responsible for xylan assembly (Brown et al., 2007; Brown et al., 2009; Lee et al., 2007; Peña et al., 2007; Wu et al., 2010; Wu et al., 2009). Lee et al. (2012) demonstrated that co-expression of IRX9 and IRX14 in tobacco BY2 cells can produce xylosyltransferase (XylT) activity but expression of either IRX9 or IRX14 alone resulted in no activity. Recently, two research groups have independently demonstrated that heterologously expressed IRX10 has processive xylan XylT activity. Urbanowicz et al. (2014) expressed *Arabidopsis IRX10-L* in mammalian HEK293 cells and Jensen et al. (2014) expressed separately a psyllium (*Plantago ovata)* and moss (*Physcomitrella patens*) *IRX10* gene in *Pichia pastoris*, finding that the heterologously expressed IRX10 proteins could add multiple Xyl residues onto a xylo-oligosaccharide acceptor. Additionally, *XXT1*, *XXT2* and *XXT5* encode XylTs that are required for xyloglucan side-chain biosynthesis (Cavalier and Keegstra,

2006; Cavalier et al., 2008; Zabotina et al., 2008). *RGXT1* and *RGXT2* encode XylTs involved in the synthesis of RG-II side-chains and *XGD1* is involved in xylogalacturonan synthesis (Egelund et al., 2006; Jensen et al., 2008). In plants, UDP-Xyl can be epimerized by UDP-Xyl 4-epimerases (UXE, EC 5.1.3.5) to UDP-L-Ara, which is used for arabinoxylan and pectin biosynthesis (Reiter and Vanzin, 2001). Thus, given the central role of UDP-Xyl in polysaccharide and glycoprotein biosynthesis, the elucidating the underlying synthesis mechanism is vital.

UDP-glucuronic acid decarboxylase (UXS) irreversibly catalyzes decarboxylation of UDP-glucuronic acid (UDP-GlcA) to form UDP-Xyl (Bar-Peled et al., 2001; Harper and Bar-Peled, 2002). The first *UXS* gene was identified from the fungus *Cryptococcus neoformans* based on sequence homology with the bacterial *ORF3* gene (*arnA*), which was hypothesized to exhibit a similar function (Bar-Peled et al., 2001). The first plant *UXS* genes were identified in *Arabidopsis* by sequence homology to the *Cryptococcus neoformans UXS* gene (Harper and Bar-Peled, 2002). Subsequently, *UXS* genes have been cloned from other plant species, including rice (*Oryza sativa*) (Suzuki et al., 2004), barley (*Hordeum vulgare*) (Zhang et al., 2005), tobacco (*Nicotiana tabaccum*) (Bindschedler et al., 2007) and Chinese white poplar (*Populus tomentosa*) (Du et al., 2013).

Previous UXS studies have mainly focused on protein expression and enzyme activities (Harper and Bar-Peled, 2002; Kobayashi et al., 2002; Suzuki et al., 2003). In plants, UXS proteins are located in the cytosol or the Golgi/ER lumen (Harper and Bar-Peled, 2002; Kobayashi et al., 2002). Bioinformatic analyses of the UXS gene sequences predict that AtUXS1, AtUXS2 and AtUXS4 have a type II transmembrane domain, whereas AtUXS3, AtUXS5 and AtUXS6 are predicted to be cytosolic (Harper & Bar-Peled, 2002). This raises questions as to the function(s) of these two groups of AtUXS enzymes *in planta*.

To date, almost all nucleotide sugar biosynthesis genes from plants have been cloned and expressed, and their catalytic activities have been established *in vitro*. In contrast, only a small number of these genes have been studied using molecular genetics techniques (Bar-Peled and O'Neill, 2011). In this study, we used reverse genetics and biochemistry approaches to analyze the functions of all six *Arabidopsis* UXS isoforms. Our results show that the cytosol UXS play a more important role than

107 the Golgi localized UXS in xylan biosynthesis.

108

RESULTS

Phylogenetic characteristics and gene expression analysis of *AtUXS* genes

To understand the evolutionary history of the *UXS* gene family in land plants, a phylogenetic tree was constructed with 39 UXS protein sequences from *Arabidopsis thaliana* (At), *Chlamydomonas reinhardtii* (Cr), *Selaginella moellendorffii (*Sm*), Physcomitrella patens* (Pp), *Picea abies* (Norway spruce; Ns), *Populus trichocarpa* (Pt), *Eucalyptus grandis* (Eg), *Oryza sativa* (Os), and *Hordeum vulgare (*Hv) (Supplemental Table 1). The phylogenetic tree shows that *UXS* genes in land plants fall into two groups (Group I and II, Supplemental Figure 1). Based on predicted transmembrane structures by TMHMM2.0 (http://www.cbs.dtu.dk/services/TMHMM/, Supplemental Figure 2 of AtUXS proteins as example), all Group I UXS proteins are devoid of transmembrane helices, whereas most of the Group II UXS proteins contain a transmembrane helix.

There are six *AtUXS* genes encoding polypeptides of between 343 to 458 amino acids in *Arabidopsis*. Group I includes AtUXS3, AtUXS5 and AtUXS6 with 92.0% amino acid identity and Group II includes AtUXS1, AtUXS2 and AtUXS4 with 76% amino acid identity (Supplemental Figure 3). All six proteins contain conserved features of the UXS family, including an N-terminal ADP-binding sequence GxxGxxG related to NAD(P)-binding and a catalytic triad of Ser, Tyr and Lys where the Tyr and Lys are in the conserved YxxxK motif (Wierenga et al., 1986; Harper and Bar-Peled, 2002). Group I proteins have the conserved amino acid sequence GGAGFVG whereas Group II proteins have the conserved amino acid sequence GGAGFIG in the NAD(P)-binding site (Supplemental Figure 3).

Quantitative PCR (qPCR) was employed to determine developmental and spatial gene expression levels of *AtUXS* genes in various organs (Supplemental Table 2 for primers). The results show that all six genes are most highly expressed in the stem, which is consistent with microarray data from *Arabidopsis* (Winter et al., 2007). Generally, gene expression levels in the Group I clade (*AtUXS3*, *AtUXS5* and *AtUXS6*) were higher than gene expression levels in the Group II clade (*AtUXS1*, *AtUXS2* and *AtUXS4*), with *AtUXS1* and *AtUXS2* exhibiting the lowest expression levels among all six genes (Supplemental Figure 4). In addition, to compare *AtUXS* expression patterns with UDP-Xyl

utilization, differential expression analysis of *IRX9* and *IRX10* (genes involved in xylan synthesis) was undertaken. Expression of these genes was also observed in stem tissue, similar to *UXS3* and *UXS6* (Supplemental Figure 4B).

Subcellular location of AtUXS proteins

To experimentally verify the sub-cellular localization of AtUXS proteins, we transformed *Arabidopsis* plants with each AtUXS isoform fused to the yellow fluorescent protein (YFP) at the C-terminus under the control of the Cauliflower mosaic virus (CaMV) 35S promoter (P35S). AtUXS1, AtUXS2 and AtUXS4 are each predicted to contain a single transmembrane domain near the N-terminus (amino acid residues 48~65, 44~61 and 44~61, respectively), indicating a type II membrane protein topology. The fluorescent signals of AtUXS1-, AtUXS2- and AtUXS4-YFP were localized to small punctate bodies that resemble the Golgi (Supplemental Figure 5A-C). In contrast, AtUXS3, AtUXS5 and AtUXS6 did not have predicted transmembrane domains, suggesting they are soluble cytoplasmic proteins. The signals for AtUXS3-, AtUXS5- and AtUXS6-YFP were diffuse and evenly distributed throughout the cytoplasm (Supplemental Figure 5D-F). In order to further confirm these findings, heterologous expression of the same constructs was performed in *Nicotiana benthamiana* leaves with a Golgi marker (G-rb CD3-968 m-Cherry) (Nelson et al., 2007). YFP fluorescent signals from AtUXS1, AtUXS2 and AtUXS4 could be observed and were found to co-localize with mCherry signals from CD3-968 in the Golgi apparatus (Figure 1A-C). In contrast, fluorescent signals from AtUXS3, AtUXS5 and AtUXS6 were diffuse and found throughout the cytoplasm, which was most apparent at the cell peripheries due to the large vacuole (Figure 1D-F). Taken together, these results indicated that AtUXS1, AtUXS2 and AtUXS4 are Golgi-located, whereas AtUXS3, AtUXS5 and AtUXS6 are cytosolic.

The catalytic activity of AtUXS *in vitro* and *in planta*

In previous studies, AtUXS1, AtUXS2 and AtUXS3 were expressed in *E. coli* and the N-terminally truncated forms of AtUXS1 and AtUXS2 showed low decarboxylase activities (Bar-Peled et al., 2001; Pattathil et al., 2005). To avoid difficulties in comparing membrane-bound and soluble proteins, only the soluble AtUXS isoforms AtUXS3, AtUXS5 and AtUXS6 were selected for expression in *E. coli* to compare catalytic properties. Full-length coding regions of *AtUXS3*, *AtUXS5* and *AtUXS6* were

cloned into the expression vector pGEX-4T (GE Healthcare), expressed in *E. coli*, and purified using the GST tag (Supplemental Figure 6).

After incubation of recombinant AtUXS3, AtUXS5 and AtUXS6 proteins with the substrate UDP-GlcA, the reaction products were separated using HPLC. As predicted, the three AtUXS proteins catalyzed UDP-GlcA conversion to a new product (Supplemental Figure 7A), which had the same retention time as the UDP-Xyl standard. ^{1}H-NMR analysis confirmed that the product was UDP-Xyl (Supplemental Figure 7B). These results demonstrate that AtUXS3, AtUXS5 and AtUXS6 are functional UDP-GlcA decarboxylases. As stated earlier, AtUXS3, AtUXS5 and AtUXS6 share over 90% amino acid identity (Supplemental Figure 3) and a comparison of their kinetic parameters revealed different affinity capabilities with UDP-GlcA among AtUXS5 (K_m=0.40 mM), AtUXS3 (K_m=0.48 mM) and AtUXS6 (K_m=0.54 mM) (Supplemental Figure 7C). The pH and temperature optima for all three isoforms were pH 6.0 (Supplemental Figure 7D) and 30°C (Supplemental Figure 7E), respectively, consistent with previously reported values (Harper and Bar-Peled, 2002).

In order to avoid technical difficulties associated with the handling of heterologously expressed transmembrane proteins in microorganisms, we used a plant-based heterologous protein expression system (*N. benthamiana*) to confirm AtUXS activity *in planta* (Jensen et al., 2008). The AtUXS5 polyclonal antibody and HA tag antibody were used together to assess protein expression levels in Group I (soluble proteins) and Group II (microsomal proteins), respectively. For each total protein extract from *N. benthamiana* leaves, similar western blot signals at a molecular weight of about 40 kDa were observed with the AtUXS5 antibody for all three Group I UXS samples (Supplemental Figure 8). A similar result at a molecular weight of about 55 kDa was obtained when the Group II UXS samples were probed with the HA antibody, indicating AtUXS protein activity could be compared independently in each group (Supplemental Figure 8). The AtUXS proteins from the two groups have different capacities to catalyze the conversion of UDP-GlcA to UDP-Xyl (Figure 2A). The enzyme activity of AtUXS proteins from Group I resulted in a significant increase in activity, with the cytosolic-localized AtUXS3 showing the highest activity (475 nmol UDP-Xyl min^{-1} mg^{-1}). The enzyme activity of the Golgi-localized AtUXS proteins (Group II) resulted in minimal activity

198 compared to the control (WT) with AtUXS2 having the lowest activity (53 nmol UDP-Xyl min^{-1}
199 mg^{-1}) in Group II (Figure 2A).
200
201 **Multiple *UXS* genes are redundant**
202 The two different subcellular locations of the AtUXS isoforms raise a question of functional
203 redundancy for these two groups in wall formation. As most non-cellulosic polysaccharides are
204 synthesized in the Golgi lumen, do the Golgi-located AtUXS isoforms play a more important role in
205 cell wall polysaccharide formation than the cytosolic AtUXS isoforms? To investigate the role of the
206 two groups of AtUXS *in vivo*, a reverse genetics approach was used. Seeds from existing T-DNA
207 insertion lines for each *UXS* gene were obtained and the resultant seedlings genotyped to select
208 homozygous individuals for further analysis (Figure 3A and Supplemental Table 3). Each T-DNA
209 insertion line corresponding to a homozygous mutant was identified by genotyping. To determine
210 whether there was any residual expression of the T-DNA-tagged *UXS* genes, an RT-PCR approach
211 was used with primers spanning the T-DNA insertion site. Our results showed that *uxs1* and *uxs5* are
212 knock-down T-DNA lines only but all others were confirmed to be knock-out lines (Figure 3B and
213 Supplemental Table 4). None of the six single *uxs* mutants showed any obvious phenotype. The
214 rosette, stem growth, flowers and fecundity were found to be similar to Col-0 plants (Supplemental
215 Figure 9).
216
217 To overcome possible functional redundancy between the *UXS* genes, we preferentially screened
218 double and triple mutant combinations of the Group I and II genes. Although the double mutants
219 maintained wild type phenotypes (Supplemental Figure 9), the triple mutant *uxs3uxs5uxs6* (Group I)
220 exhibited delayed growth, a darker leaf colour, shorter stems and smaller flowers under long (16 h)
221 day conditions (Figure 3C, D). In contrast, the triple mutant *uxs1uxs2uxs4* (Group II) displayed a less
222 severe phenotype than *uxs3uxs5uxs6* (Group I) and was more similar to wild type (Figure 3C, D).
223
224 UXS enzyme activity in whole cell extracts was measured between the two triple mutant lines and
225 wild type. Approximately 65% of the wild type level of UXS activity was observed in *uxs1uxs2uxs4*
226 (Group II) whereas *uxs3uxs5uxs6* (Group I) only retained 25% of wild type UXS activity (Figure 2B).

These results suggest that the cytosolic AtUXS isoforms might supply a larger fraction of the UDP-Xyl pool and therefore may be more essential for plant growth.

Secondary cell walls is decreased in the UXS triple mutants

To explore whether the various observed phenotypes were caused by a defect in secondary cell walls, transverse sections of stems for each mutant line were examined by light and transmission electron microscopy. None of the six single *uxs* mutants showed abnormal morphologies (Supplemental Figure 10). Similarly, the *uxs1uxs2uxs4* mutant displayed normal vascular bundle morphology. However, a striking phenotype was observed in the *uxs3uxs5uxs6* triple mutant stems, where a collapse of xylem vessels and reduced thickness of fiber cells and xylem vessel walls occurred when compared with the wild type (Figure 4A-F). The thickness of interfascicular fiber cell walls of the *uxs3uxs5uxs6* mutant was only 0.80 μm compared with the wild type (1.74 μm) and the *uxs1uxs2uxs4* mutant (1.34 μm) (Figure 4G-I). The *uxs3uxs5uxs6* phenotype is reminiscent of the irregular xylem (*irx*) phenotype suggesting that xylan synthesis in this mutant was severely impacted (Brown et al., 2005).

Cell wall composition in *uxs* mutants

To examine the effect of *uxs* mutations on the cell wall, non-cellulosic monosaccharide composition of AIR from stem material of the wild type and triple mutants was determined. We observed minimal differences in the monosaccharide composition of stem material between the wild type and *uxs1uxs2uxs4* (Group II) mutant (Table 1). In contrast, the levels of Xyl in cell wall extracts from the *uxs3uxs5uxs6* (Group I) mutant were significantly lower, exhibiting a 21% decrease. We also observed a significant decrease in GlcA levels (42%) in the *uxs3uxs5uxs6* triple mutant as well as a two-fold increase in the amount of Ara (Table 1). These data indicate that cytosolic UXS is important for the biosynthesis of Xyl- and GlcA-containing cell wall polysaccharides. These findings are consistent with the recent characterization of a UDP-Xyl transporter (UXT) transferring UDP-Xyl from the cytoplasm into the Golgi lumen for xylan biosynthesis (Ebert et al., 2015).

AIR from the inflorescence stems were also subjected to linkage analysis to assess polysaccharide composition in the triple mutants (Supplemental Table 5). The predominant polysaccharides in the

cell walls from stem material were cellulose and heteroxylans with low amounts of heteromannans, xyloglucans and pectic polysaccharides (Supplemental Table 5). Heteroxylan content decreased by approximately 30% in *uxs3uxs5uxs6* (Group I) mutant stems (17.4 mol%) compared with the wild type (25.1 mol%). As expected, no obvious change was observed in heteroxylan content in the *uxs1uxs2uxs4* (Group II) triple mutant. Cellulose content decreased in both *uxs1uxs2uxs4* and *uxs3uxs5uxs6* triple mutants, while the level of xyloglucan in both mutants showed no significant difference in the stem material compared to WT (Supplemental Table 5). Finally, the content of pectic polysaccharides approximately doubled in both the mutants [from 7.6 (wild type) to 17.7 (*uxs1uxs2uxs4)* and 19.8 (*uxs3uxs5uxs6)* mol%, respectively], showing pleiotropic effects as previously observed when there have been attempts to modify the composition of plant cell walls (Doblin et al., 2014). The results indicate that cytosolic UXS might affect heteroxylan biosynthesis by regulating UDP-Xyl substrate concentrations.

The LM10 monoclonal antibody (McCartney et al., 2005) was used to investigate heteroxylan distribution in mutant stems. In wild type plants, the strongest fluorescence signals were detected in the cell walls of xylem cells and interfascicular fibers. A weaker signal was detected in the *uxs3uxs5uxs6* triple mutant with this probe (Supplemental Figure 11). This result corroborates our linkage analysis, indicating that *uxs3uxs5uxs6* deposits less xylan in the stem compared to the wild type.

Xylan structure analysis in triple *uxs* mutants

In most xylan-related mutants such as *irx9*, *irx10*, *irx14*, an increase in the proportion of MeGlcA to GlcA is observed (Brown et al., 2007; Brown et al., 2009; Lee et al., 2007; Peña et al., 2007; Wu et al., 2010; Wu et al., 2009). Therefore, the levels of GlcA and MeGlcA, which constitute the major side chain on *Arabidopsis* xylan, were analyzed in wild type and the *uxs1uxs2uxs4* and *uxs3uxs5uxs6* triple mutants. MALDI-TOF MS spectra showed the expected prominent pseudo-molecular ion peaks (*m/z*) 745, 759, 767, 781 and 797 could be attributed to GlcA-Xyl_4-Na^+, MeGlcA-Xyl_4-Na^+, Gal-GlcA-Xyl_3-Na^+, GlcA-Xyl_4-$2Na^+$, MeGlcA-Xyl_4-$2Na^+$ and Gal-GlcA-Xyl_3-$2Na^+$ (Zhong et al., 2005; Zhong et al., 2014), respectively (Figure 5). Comparing the peak areas of the pseudo-molecular ions MeGlcA/(MeGlcA+GlcA) in *uxs1uxs2uxs4* and *uxs3uxs5uxs6*, the proportion

was determined to be 87.9% and 96.1%, respectively, showing an increase of 8.8% and 17.0%, respectively, compared to wild type (79.1%). The Gal-GlcA-Xyl_3 pseudo-molecular ions only represent a small proportion of the total measured GlcA and were therefore not considered. These data indicate that the *uxs* triple mutants respond in a manner similar to the xylan-related *irx* mutants.

Molecular weight of non-cellulosic polysaccharide in *uxs* triple mutants

Our data have shown that there is a discernible reduction in xylan content in the *uxs3uxs5uxs6* triple mutant (Supplemental Table 5). Thus, we examined whether the molecular size distribution of the non-cellulosic polysaccharides, which is mainly xylan in the stem, was also affected in the *uxs* triple mutants. The molecular weight of non-cellulosic polysaccharide fractions from wild type, *uxs1uxs2uxs4* and *uxs3uxs5uxs6* triple mutants were analyzed by gel permeation chromatography (GPC) in 1 N and 2 N KOH extracted fractions. A significant decrease in molecular weight was found in both triple mutants (Table 2). For non-cellulosic polysaccharides extracted in 1 N KOH, the weight-average molecular weight (M_w) and number-average molecular weight (M_n) of non-cellulosic polysaccharides in the *uxs3uxs5uxs6* mutant is 24.3 kDa and 9.7 kDa, respectively, both of which are significantly reduced compared to wild type (Table 2). An intermediate M_w value between wild type and *uxs3uxs5uxs6* was observed for *uxs1uxs2uxs4*. M_w values are higher for all three lines in the 2N KOH extracted fractions with *uxs1uxs2uxs4* and *uxs3uxs5uxs6* showing a similar M_w reduction trend compared to wild type. However, all three lines have similar M_n values in 2N KOH compared to 1N KOH fractions in which both mutants displayed reduced values. The results indicate that the non-cellulosic polysaccharide backbone length is significantly reduced in both the *uxs* triple mutants, with *uxs3uxs5uxs6* having the greatest size reduction of the two mutants.

The *uxs* triple mutants exhibit improved sugar release after saccharification

The altered cell wall composition and morphology of *uxs* triple mutants prompted us to examine the effect they might have on cell wall digestibility. Consequently, the *uxs3uxs5uxs6* triple mutant showed improved glucose release of up to 18% (Figure 6). Surprisingly, with lower xylose content, the *uxs3uxs5uxs6* triple mutant also showed increased release of xylose. The reason may be similar to what was observed in the *irx9* and transformant lines as shown by Petersen et al. (2012), which exhibited higher xylose released compared with the wild type line. Xylan is more accessible to

317 enzymatic breakdown in the *uxs3uxs5uxs6* triple mutant. The *uxs1uxs2uxs4* triple mutant showed no
318 difference compared to the wild type, which was consistent with less change in the phenotype and
319 monosaccharide composition.
320

DISCUSSION

Compartmentalisation of *UXS* genes

Comprehensive studies of gene expression provide useful information for predicting gene function. Previously, qPCR data illustrated that *Arabidopsis UXS* genes are mainly expressed in the stems, as are the xylan backbone and side-chain synthesis genes (Supplemental Figure 4) (Brown et al., 2009; Lee et al., 2010; Wu et al., 2010; Wu et al., 2009). Thus, the enhanced xylan deposition observed in stems could be supported by the increased level of UDP-Xyl produced by increased expression of *UXS* genes. AtUXS1, AtUXS2 and AtUXS4 (Group II, Supplemental Figure 3) each have a type II membrane protein topology and are located in the Golgi lumen (Figure 1). In contrast, the second UXS clade that includes AtUXS3, AtUXS5 and AtUXS6 (Group I), contain no predicted transmembrane domains and are located in the cytosol (Figure 1 and Supplemental Figure 5). The expression levels of Group I members (AtUXS3, AtUXS5 and AtUXS6) in the stem are generally higher than the levels of Group II members (AtUXS1, AtUXS2 and AtUXS4) (Supplemental Figure 4). This finding further highlights the potential importance of cytosolic derived UDP-Xyl in cell wall biosynthesis.

The cell wall XylTs are located in the secretory pathway, mainly in the lumen of the Golgi apparatus and are involved in the biosynthesis of xylan (IRX9, IRX10, IRX14; (Jensen et al., 2014; Lee et al., 2012), xyloglucan (XXT1, XXT2 and XXT5; (Ahn et al., 2006), and RG-II (RGXT1, RGXT2, RGXT3 and RGXT4 (Egelund et al., 2008; Liu et al., 2011). The subcellular localization of these XylTs and the presence of Golgi-located UXS enzymes would indicate a central role for lumenal UDP-Xyl. Recently, a family of three Golgi-located UDP-Xyl transporters (UXTs) were characterized in *Arabidopsis* (Ebert et al., 2015). Moreover, *UXT1* mutant analysis indicated a reduction in cell wall-derived Xyl from stem material and an apparent role in the biosynthesis of glucuronoxylans (Ebert et al., 2015). Thus, the transport of cytosolic UDP-Xyl into the Golgi lumen likely plays an essential role in providing substrates for xylan, and potentially xyloglucan and pectic polysaccharide biosynthetic enzymes (Figure 7).

Plant genomes and EST sequences reveal the diversity of *UXS* genes *in planta* (Supplemental Figure 1). Compared with other land plant genera, there are only two *UXS* genes in Norway spruce (*Picea abies)*. Based on sequence analysis, one UXS appears to be located in the cytosol and the other in the Golgi. This is possibly because heteromannans, not heteroxylans, are the major non-cellulosic polysaccharides in gymnosperms. A phylogenetic tree reveals that all UXS members in Group I have no predicted transmembrane helices. However, in Group II, a majority of proteins have a predicted transmembrane helix except four members (EgUXS4, OsUXS2, OsUXS5 and HvUXS3). Interestingly, there is only one Group I member in *Physcomitrella patens*, barley and rice, but in dicot species with well-developed vasculature such as *Arabidopsis*, *Populus trichocarpa* and *Eucalyptus grandis*, there are multiple Group I UXS members. This may be because these species require more cytosolic-synthesized UDP-Xyl for xylan biosynthesis. Further work is needed in *Arabidopsis* and other species to more precisely describe the functions of the membrane-bound versus cytosolic UXS isoforms.

Cytosolic *UXS* genes are redundant and essential for plant development

The three cytosolic AtUXSenzymes (AtUXS3, AtUXS5, AtUXS6) exhibited differential kinetic properties when expressed in *E. coli* with AtUXS3 showing the highest activity, as previously shown (Harper and Bar-Peled, 2002). In contrast, the lumenal AtUXS enzymes (AtUXS1, AtUXS2, AtUXS4) demonstrated a significant decrease in relative activity compared to the cytosolic isoforms when heterologously expressed in *N. benthamiana* (Figure 2A). These observations are similar to previous findings when comparing *in vitro* activities of the lumenal isoforms AtUXS1 and AtUXS2 with AtUXS3 (Harper and Bar-Peled, 2002). A more recent analysis of AtUXS2 activity indicated that it has an apparent K_m of 0.2 mM, although this study was undertaken with an N-terminally truncated protein (Pattathil et al., 2005). Given the problems associated with assessing membrane-associated enzyme activities, it is unclear whether such distinct differences in activity between the cytosolic and lumenal AtUXS enzymes exist.

While enzyme activities for *E. coli*-expressed AtUXS1, AtUXS2 and AtUXS3 have been previously reported (Harper and Bar-Peled, 2002; Pattathil et al., 2005), there are no reports on AtUXS enzyme function *in vivo*. Employing reverse genetics approaches, we found that single and double *uxs*

mutants exhibit wild type phenotypes, implying some level of functional redundancy (Supplemental Figure 9). As a consequence, we generated triple mutant lines based on the two functional AtUXS sub-groups. The triple mutant, *uxs1uxs2uxs4* comprising Group II members, resulted in no obvious phenotype. In contrast, the *uxs3uxs5uxs6* triple mutant comprising Group I members resulted in a severe phenotype with delayed growth, darker leaf color and a high proportion of irregular xylem vessels (Figure 3 and 4). This type of phenotype is very similar to the well-characterized xylan-defective mutants *irx7, irx8, irx9, irx10* and *parvus* (Brown et al., 2009; Wu et al., 2009). These results indicate that collectively, the cytosolic AtUXS isoforms are likely essential for the synthesis of xylan in stems. Finally, endogenous UXS activity in the triple mutants supported *in vitro* activity data, indicating that cytosolic AtUXS enzymes are more active than the luminal AtUXS enzymes.

While cytosolic AtUXS enzymes are likely to produce the majority of cytosolic UDP-Xyl, a cytosolic UDP-Api/UDP-Xyl synthase (AXS) also exists that is able to convert UDP-GlcA into both UDP-Xyl and UDP-Api (Figure 7) with an Api/Xyl ratio of 0.6 (Molhoj et al., 2003). These two *AtAXS* genes are highly expressed in all plant organs (Ahn et al., 2006; Molhoj et al., 2003) and are proposed to contribute to the assembly of RG-II side chains B and A, which contain D-Api (Ahn et al., 2006). Since Api is only present in the pectic polysaccharide RG-II (Stevenson et al., 1986), which is present in very low abundance, the amount of cytosolic UDP-Xyl produced by AXS is likely to be limited. Thus, the major pool of cytosolic UDP-Xyl is likely produced by UXS. This hypothesis is consistent with previous reports about *AXS* only affecting RGII synthesis in tobacco (Ahn et al., 2006).

Lack of UXS activity leads to altered xylan

Employing chemical analyses and immunocytochemistry, we found that xylan derived from *Arabidopsis* stems was altered in abundance and molecular weight in the triple mutants when compared to wild type (Tables 1 to 3). The xylan backbone synthesis genes *IRX9* and *IRX9-L, IRX14* and *IRX14-L*, and *IRX10* and *IRX10-L* are redundant pairs, with the "like (L)" genes being minor isoforms (Brown et al., 2007; Brown et al., 2009; Chiniquy et al., 2013; Keppler and Showalter, 2010; Lee et al., 2007; Peña et al., 2007; Wu et al., 2010). This redundancy is linked to activity differences

and suggests that xylan synthesis is dosage-dependent and rate-limited (Peña et al., 2007). UDP-Xyl is the main substrate for xylan synthesis, with Xyl residues constituting the entire backbone of this polysaccharide. We propose that UDP-Xyl concentration might decrease in *uxs* triple mutant plants and that this reduction in substrate availability for xylan biosynthesis results in reduced backbone elongation during fast growth of the stem. Although cytosolic-derived UDP-Xyl appears to be the main substrate source for xylan biosynthesis, the reduced molecular weight of xylan observed in the *uxs1uxs2uxs4* triple mutant also supports a contribution by lumenal UXS to the UDP-Xyl pool for xylan biosynthesis. Thus, the reduced M_w of xylan in *uxs1uxs2uxs4* and *uxs3uxs5uxs6* indicates that the quantity of donor UDP-Xyl generated by both the Golgi and cytosolic UXS isoforms might be important in controlling xylan chain length.

The increased ratio of methylglucuronic acid (MeGlcA) to non-methylated GlcA is a common feature of all known xylan-deficient mutants (Zhong et al., 2005), a feature also observed in both the cytosolic and Golgi *UXS* triple mutant plants. 4-*O*-Methylation of GlcA is catalyzed by glucuronoxylan methyltransferase (GXMT), which was classified as a domain of unknown function (DUF) 579 protein (Urbanowicz et al., 2012). In wild-type *Arabidopsis*, on average a side branch is added to one in eight Xyl residues with an Me-GlcA to GlcA ratio of two (Brown et al., 2007). Detailed analyses of xylan mutants indicate that while the proportion of non-methylated GlcA decreases, the overall amount of MeGlcA tends to remain the same (Ebert et al., 2015). These findings indicate that while xylan levels can be reduced, there is a requirement for a certain proportion of MeGlcA to be present in the cell wall.

Interestingly, IRX15 and IRX15L appear to affect xylan length with the *irx15irx15L* double mutant displaying enhanced saccharification capacity (Brown et al., 2011). Similar results were obtained with the triple mutants, *uxs1uxs2uxs4* and *uxs3uxs5uxs6* (Figure 6). Since xylan length contributes to recalcitrance of ligno-cellulosic biomass, it is possible that the lower DP xylan would make the walls of the triple mutants more degradable.

METHODS

Phylogenetic and Sequence Analysis of *UXS* Genes

Amino acid sequences of the *UXS* genes were obtained from UniProt (UniProt Consortium, 2015). Sequence identities were determined using DNAMAN software version 8 (Lynnon Biosoft). Sequences were aligned using the Clustal MUSCLE program (Edgar, 2004) with default parameters. Phylogenetic trees were generated using the Neighbor-Joining method and bootstrap values generated from 1,000 replicates. Prediction of transmembrane helices was conducted using TMHMM v.2.0 (Krogh et al., 2001).

Plant growth conditions

Seeds were surface sterilized in 10% NaOCl with 1% (v/v) Tween-20 (v/v), vortexed five times for 10 min, washed three times in ultrapure water before 75% ethanol was added for 1 min, followed by three washes with sterilized water. Sterile seeds were sown on MS medium plates (4.4 g Murashige and Skoog basal salt mixture, pH 5.8, containing 1% (w/v) sucrose). The plates were refrigerated at 4°C in darkness for 2 d before transfer to a controlled environment growth cabinet (23°C, 60% humidity, 100-120 $\mu mol \cdot m^{-2} \cdot s^{-1}$, 16 h light/8 h dark). Seedlings were transferred to soil 10-d later for plant morphological analysis.

Plant material and identification of homozygous mutants

All *AtUXS* T-DNA insertion lines were obtained from the Arabidopsis Biological Resource Center (ABRC, https://abrc.osu.edu/) including *uxs1* (N555603, Salk_055603, sixth intron), *uxs2* (N503691, Salk_003691, first exon), *uxs3* (N907654, WiscDsLoxHs080_09, fifth exon), *uxs4* (N609630, Salk_109630, fifth intron), *uxs5* (N850623, WiscDsLox293-296invD4, eighth intron) and *uxs6* (N678548, salk_058602, second intron) (Figure 4A). The homozygous *uxs* combination mutants were obtained by genetic crosses. Homozygous T-DNA insertion mutants were identified by PCR of genomic DNA. Primers used for this purpose are listed in Supplemental Table 3.

Quantitative PCR (qPCR) analysis

Total RNA of wild type *Arabidopsis* was extracted with a plant total RNA extraction kit (Omega, USA) and treated with DNase I (BioRad, USA). The first-strand cDNA was synthesized with a TAKARA cDNA synthesis kit (Cat#6130, Japan) according the manufacturer's protocol. Total RNA was extracted from 10 d-old shoots, 3-week-old rosette leaves, full-opened flowers and 10 d-old siliques from 5-week-old plants, top, middle and bottom part of 7-week-old stem (in flower) and 2-week-old roots of wild type plants. Primers for qPCR analysis were designed according to the *AtUXS* gene sequences, and only primers efficiencies for amplification were more than 92% listed for further analysis (Supplemental Table 2). Relative qPCR was performed according the method of Schmittgen and Livak (2008).

Transcript Analysis by RT-PCR

For determining *UXS* gene expression, total RNA from 2-week-old seedlings in *uxs* mutants and wild type were extracted and treated using the methods listed above. The *AtUXS* transcripts were analyzed by PCR using the primers as listed in Supplemental Table 4. PCR included an initial heating step (5 min, 94°C), followed by 36 cycles consisting of denaturation (25 s, 94°C), annealing (25 s, 55°C), and extension (50 s, 72°C), and a final incubation at 72°C for 10 min. PCR products were separated on a 2% (w/v) agarose gel in TAE buffer. As a control, the 18s RNA was amplified for 24 cycles (primers in Supplemental Table 4).

Stem sectioning

Stem segments were cut at a height of 3 cm from the rosette of 8-week-old with full siliques soil-grown plants and then embedded in 3% (w/v) agarose (BioWest, Spain). Sections (50 μm) were then cut with a VT1000S vibratome (Leica, Germany). The sections were stained with 0.02% toluidine blue O (Sigma-Aldrich) for 30 s to 1 min, washed with water and then observed under a light microscope (Olympus BX43F, Japan). Stem segments from 3 independent plants were collected, and >10 sections were viewed per plant.

Transmission Electron Microscopy

Stem segments were cut from the bottom part of 8-week-old with full siliques soil-grown plants and then vacuum infiltrated in 4% (v/v) glutaraldehyde in PBS (33 mM Na_2HPO_4, 1.8 mM NaH_2PO_4 and

140 mM NaCl, pH 7.2) before being fixed in 2% glutaraldehyde in PBS at 4°C overnight. After fixation, tissues were post-fixed in 1% (w/v) osmium tetroxide and then dehydrated through a gradient of ethanol and embedded in Spurr's resin. Sections (70-100 nm) were stained with uranyl acetate and lead citrate and visualized using an FEI Tecnai 12 transmission electron microscope. Finally cell wall thickness was measured from 8 cells on each section with three technical repeats using FEI microscopy software Gatan Digital Micrograph.

Immunolocalization analysis of heteroxylans in mutants

Sections were washed with 0.1 M PBS buffer (0.1 M PBS, 0.5 M NaCl, pH 7.2), then incubated with 3% (w/v) skim milk powder in PBS for 2 h. LM10, which can bind to unsubstituted and relatively low-substituted heteroxylans but not to wheat arabinoxylan (McCartney et al., 2005), was diluted 1/20 with 0.1 M PBS buffer and incubated for 4 h at room temperature. Sections were then washed with PBS buffer (five times) before secondary antibody (fluorescein isothiocyanate-conjugated, 1/50 dilution; Abcam, http://www.Abcam.com) was added. After incubation for 1 h at room temperature the sections were washed a further five times and the immunofluorescence observed on a Zeiss LSM710 confocal microscope.

Subcellular location of AtUXS

Gateway primers (Supplemental Table 6) containing *attB* site were designed for amplification of *AtUXS* genes. The PCR products without stop codons were cloned into the pDONR207 vector by BP reaction (Life Technologies, USA) and sequenced. Verified clones were transferred into the pEarleyGate 101 destination vector (Earley et al., 2006) to produce the C-terminal YFP fusion constructs. Each of pEarlyGate101-*AtUXS* constructs were transformed into *Agrobacterium tumefaciens* strain C58. pEarlyGate101-*AtUXS* in C58 were infiltrated into *Nicotiana benthamina* as previously described (Sparkes et al., 2006). YFP signal was observed under an excitation wavelength of 514 nm and an emission wavelength of 510-545 nm. The *AtUXS3*, *AtUXS5* and *AtUXS6* constructs were co-infiltrated with the soybean α-mannosidase-mCherry (G-rb CD3-968) Golgi marker (Nelson et al., 2007) which was visualized using excitation wavelength 587 nm and emission wavelength 610 nm, to verify the location of the three proteins.

Expression of soluble AtUXS3, AtUXS5 and AtUXS6 in *E. coli*

Cytosolic At*UXS* genes were cloned into pGEX-4T by digestion and ligation at X*ho*I and E*co*RI sites with primers listed in Supplemental Table 6 and confirmed by sequencing. pET-4X-At*UXS* constructs were introduced into *E. coli* strain BL21 via electroporation. Cultures were grown at 37°C to OD_{600}=0.6 and IPTG added to a final concentration of 0.5 mM. After 3 h of induction, the cells were pelleted by centrifugation at 6,000 x g for 10 min, 4°C and resuspended in 10 mL of extraction buffer (50 mM Tris·HCl, pH 7.4, 10% glycerol, 1 mM EDTA) with fresh 1 mM DTT and 0.5 mM PMSF. The solution was lysed by sonication using a 10 s pulse followed by 20 s rest on ice, then collected and proteins purified as previously described (Bar-Peled and Raikhel, 1996). Finally, purified protein was centrifuged in a Amicon-Ultra-15 filter (MWCO10KD) at 4 °C, 4000 x g for 45 min and filtered twice with Tris·HCl pH 7.4 buffer. Protein content was calculated with the Bradford protein assay (BioRad, USA).

Western blotting analysis

The purified GST-UXS5 protein was collected and injected into three rabbits to obtain optimized polyclonal antibodies at Beijing Protein Innovation (BPI) (www.proteomics.org.cn/). pEarlyGate101-*AtUXS* in C58 was infiltrated into *N. benthamiana* as previously described (Sparkes et al., 2006). Western blotting was performed essentially as previously described (Tamura et al., 2005). The tobacco leaves were excised and ground on ice in 3 mL of 20 mM Tris·HCl pH 7.4 buffer with proteinase inhibitor cocktail (Roche, Switzerland). The homogenate was filtered using cheesecloth and centrifuged at 4000 x g, 30 min at 4°C to remove cellular debris. The supernatant, including soluble proteins and microsomal proteins, was used for Western blotting and to measure enzyme activity. In Western blotting, the protein extract buffer included 2% triton X100. The total protein extracts were: 80 μg loaded in lanes of AtUXS3, AtUXS5, AtUXS6, and 160 μg loaded in lanes of UXS1, UXS2 and UXS4. The anti-UXS5 polyclonal antibodies were used to detect UXS3, UXS5 and UXS6 (1:100 dilution), but do not detect the membrane-bound UXS isoforms. The anti-HA antibody (Sigma-Aldrich, USA) was used to detect UXS1, UXS2 and UXS4 at 1:1000 dilution. Blots were washed and then incubated with anti-mouse IgG coupled to alkaline phosphatase (Sigma-Aldrich, USA) at a dilution of 1:5000 and developed according to the manufacturer's instructions.

557

558 **AtUXS activity assays**

559 AtUXS activity assays were performed as previously described (Bar-Peled et al., 2001; Zhao et al.,
560 2014). Briefly, 50μL standard reaction mixture containing 80 mM Tris·HCl, pH 7.4, 1 mM NAD^+, 1
561 mM UDP-GlcA and 10 μg protein were incubated at 25°C for 2 h. Reactions were terminated by the
562 addition of 50 μL phenol:chloroform (1:1; v/v), vortex-mixed, and subjected to centrifugation
563 (10,000 x g, 5 min). The upper phase was retained and 100 μL ultrapure water was added to
564 re-extract the lower phase. The upper phases were mixed and analyzed by HPLC using a
565 COSMOSIL C18-AR-II column (4.6 mm × 250 mm; Nacalai Tesque, Kyoto, Japan) run at 1 mL
566 min^{-1} and monitored for UV absorbance (Agilent 1100 HPLC systems, Sig_{260nm}, Ref_{360nm}). Buffer A
567 contained 20 mM triethylamine-acetate (pH 7) and buffer B contained 20 mM triethylamine-acetate
568 mixed with 10% (v/v) acetonitrile. The gradient was 0 to 15 min (0% B), 15.1 to 30 min (15% B) and
569 post-run time 5 min (Rosenberger et al., 2012).

570

571 **Cell wall extraction and linkage analysis**

572 The bottom section of stems (5cm length from base) of 8-week-old, with maturing siliques, wild type,
573 *uxs1uxs2uxs4* and *uxs3uxs5uxs6* triple mutants were collected and ground with a mortar and pestle in
574 liquid N_2. Alcohol insoluble residue (AIR) were prepared by extraction of the powder with 96% (v/v)
575 ethanol at 70°C for 30 min and the insoluble fraction used for measurement of both neutral and
576 acidic monosaccharide linkage composition as previously described (Pettolino et al., 2012).

577

578 **Gel permeation chromatography of non-cellulosic polysaccharides**

579 Non-cellulosic polysaccharides were sequentially extracted from AIR samples (outlined above) with
580 1 N and 2 N KOH at 50°C for 3 h. The KOH extracts were neutralized with acetic acid to pH 5.5 and
581 then precipitated in three volumes of 95% ethanol. The precipitates were collected by centrifuging at
582 3, 000 x g for 5 min and washed with acidified 70% ethanol and then freeze-dried. The molecular
583 weight was determined by gel permeation chromatography-multi angle laser light scattering
584 (GPC-MALLS) methods. GPC-MALLS measurements were carried out on a DAWN HELEOS-II
585 laser photometer (Wyatt Technology Co., USA), combined with an PL aquagel-OH 50 column
586 (300×7.7 mm, Polymer Laboratories Ltd. USA, 45□) and equipped with a Model 600 pump HPLC

587 system (Waters, USA) and a Optilab rEX differential refractive index detector (Wyatt Technology
588 Co., USA). The eluent was 0.02 N NaCl in 0.005 M sodium phosphate buffer (pH 7.5) with flow rate
589 of 0.5 mL min^{-1}. Non-cellulosic polysaccharides were dissolved with the eluent buffer at a
590 concentration of 1.0 mg mL^{-1} and filtered using a 0.42 μm microfiltration membrane.
591
592 **Determination of monosaccharide composition**
593 AIR was extracted from stem material (as outlined above) and hydrolyzed in 2 N trifluoroacetic acid
594 (TFA) for 1 h at 120°C according to previous methods (Ebert et al., 2015). Sugars were separated
595 and quantified by high performance anion exchange chromatography (HPAEC) with pulsed
596 amperometric detection (PAD) as described (Øbro et al., 2004) on a Dionex ICS 3000 (Dionex) using
597 a CarboPac PA1 anion exchange column (3×150 mm; Dionex).
598
599 **Matrix-Assisted Laser Desorption Ionization-Time-Of-Flight-Mass Spectrometry**
600 **(MALDI-TOF MS)**
601 MALDI-TOF MS was performed on KOH extracts (as outlined above) and analysed as described
602 (Zhong et al., 2005). Xylan oligosaccharides were generated by *endo-β*-xylanase M6 (Megazyme)
603 digestion, then analyzed by MALDI-TOF MS with a Bruker microFLEX MALDI-TOF MS operated
604 in the positive-ion mode with an accelerating voltage of 30 kV, an extractor voltage of 9 kV, and a
605 source pressure of about 8×10^{-7} torr. The matrix was prepared by mixing saturated
606 2,5-dihydroxybenzoic acid (DHB) in 50% aqueous acetonitrile. The typical spectra shown represent
607 the sums of 200 laser shots. MeGlcA content is calculated by the peak areas of ((MeGlcA)-Xyl_4 and
608 (MeGlcA)-Xyl_4) / total (GlcA)-Xyl_4.
609
610 **Saccharification**
611 A 6 cm piece from the base of the stems of 8-week-old *Arabidopsis* were collected and ground using
612 a PM100 Ball Mill (Retsch, German). Saccharification was undertaken following cell wall
613 pretreatment by autoclaving for 30min at 120°C and using the modified procedure of Petersen et al.
614 (2012). For enzymatic saccharification, a mixture of 5 mg/mL tetracycline and 2 mg/mL
615 mixed-cellulase containing β-glucanase (3.7×10^{4}U), cellulase (3.4×10^{2}U) and xylanase (6.5×10^{4}U)
616 (Imperial Jade Bio-Technology Co., China) in 0.1 M citrate buffer, pH 5.0 was added to the

617 pretreated samples, followed by incubation at 50°C for 24 h at 100 rpm. The monosaccharide
618 products were determined by HPLC using a SP-0810 Shodex SUGAR column coupled to a refractive
619 index detector. Degradation products were detected using a UV detector (Yu et al., 2010).
620

Funding

This work was supported by Science and Technology Planning Project of Guangdong Province (Grant Number 2015A050502045), National Natural Science Foundation of China (Grant Number 31170165 and 31270594), Ministry of Science and Technology of China (Grant Number 2013AA102705, 2013BAD22B01), Guangdong Natural Science foundation (Grant Number S2013010011988), ARC Centre of Excellence in Plant Cell Walls, Australia (Grant Number CE110001007).

Author Contributions

K. B., C. X. and W.A. designed research; K. B., Z. X., Z. C., Z. W., R. J., E. B., B. C.T., D. X., Z. Q., and Z. G.. performed research; D. M.S., H. J.L., B. A., C. X., and W. A. analyzed data; K. B., B. A, and W.A. wrote the paper

Acknowledgements

We thank Jing Fan, Chunxu Ni and Haoyang Fu for their help in protein expression in *E. coli*. All pEarlyGate vectors, Golgi marker (CD3-968) and *Arabidopsis uxs* mutants were provided by ABRC at Ohio State University (www.arabidopsis.org). C. B, W. Z, M.S.D and A.B acknowledge support of the ARC Centre of Excellence in Plant Cell Walls (CE110001007).

Supplemental data

Supplemental Table 1. The abbreviate genes name were shown with correspondent gene number in NCBI database.

Supplemental Table 2. qPCR primers for expression pattern

Supplemental Table 3. T-DNA primers

Supplemental Table 4. RT-PCR Primers

Supplemental Table 5. Linkage analysis (mol%) from AIR of stem extracts of wild type (Col-0) and the *uxs1uxs2uxs4* and *uxs3uxs5uxs6* triple mutants.

Supplemental Table 6. Cloning primers

Supplemental Figure 1. Phylogenetic tree of UXS proteins in land plants.

Supplemental Figure 2. TMHMM2.0 program predict AtUXS transmembrane helices.

651 Supplemental Figure 3. Alignment of amino acid sequences of *Arabidopsis thaliana* UXS proteins.

652 Supplemental Figure 4. Expression patterns of the *AtUXS1-6* genes in different organs at different
653 development stages.

654 Supplemental Figure 5. The AtUXS-YFP fluorescent signals in *Arabidopsis* root epidermal cells.

655 Supplemental Figure 6. Expression of UXS5 in *E. coli*.

656 Supplemental Figure 7. Enzyme activity and characterization of recombinant soluble AtUXS
657 isoforms.

658 Supplemental Figure 8. Expression of AtUXS in tobacco leaves

659 Supplemental Figure 9. Five-week-old rosettes of single and double *UXS* mutants.

660 Supplemental Figure 10. Transverse sections of vascular tissue of single mutants.

661 Supplemental Figure 11. Immunolocalisation of the LM10 epitope in stem tissues.

662

References

Ahn, J.W., Verma, R., Kim, M., Lee, J.Y., Kim, Y.K., Bang, J.W., Reiter, W.D., and Pai, H.S. (2006). Depletion of UDP-D-apiose/UDP-D-xylose synthases results in rhamnogalacturonan-II deficiency, cell wall thickening, and cell death in higher plants. J. Biol. Chem. 281:13708-13716.

Bar-Peled, M., Griffith, C.L., and Doering, T.L. (2001). Functional cloning and characterization of a UDP- glucuronic acid decarboxylase: the pathogenic fungus *Cryptococcus neoformans* elucidates UDP-xylose synthesis. Proc. Natl Acad. Sci. USA 98:12003-12008.

Bar-Peled, M., and O'Neill, M.A. (2011). Plant nucleotide sugar formation, interconversion, and salvage by sugar recycling. Annu. Rev. Plant Biol. 62:127-155.

Bar-Peled, M., and Raikhel, N.V. (1996). A method for isolation and purification of specific antibodies to a protein fused to the GST. Anal. Biochem. 241:140-142.

Bindschedler, L.V., Tuerck, J., Maunders, M., Ruel, K., Petit-Conil, M., Danoun, S., Boudet, A.M., Joseleau, J.P., and Bolwell, G.P. (2007). Modification of hemicellulose content by antisense down-regulation of UDP-glucuronate decarboxylase in tobacco and its consequences for cellulose extractability. Phytochemistry 68:2635-2648.

Brown, D.M., Goubet, F., Wong, V.W., Goodacre, R., Stephens, E., Dupree, P., and Turner, S.R. (2007). Comparison of five xylan synthesis mutants reveals new insight into the mechanisms of xylan synthesis. Plant J. 52:1154-1168.

Brown, D.M., Zeef, L.A., Ellis, J., Goodacre, R., and Turner, S.R. (2005). Identification of novel genes in Arabidopsis involved in secondary cell wall formation using expression profiling and reverse genetics. The Plant cell 17:2281-2295.

Brown, D.M., Zhang, Z., Stephens, E., Dupree, P., and Turner, S.R. (2009). Characterization of IRX10 and IRX10-like reveals an essential role in glucuronoxylan biosynthesis in Arabidopsis. Plant J. 57:732-746.

Cavalier, D.M., and Keegstra, K. (2006). Two xyloglucan xylosyltransferases catalyze the addition of multiple xylosyl residues to cellohexaose. J. Biol. Chem. 281:34197-34207.

Cavalier, D.M., Lerouxel, O., Neumetzler, L., Yamauchi, K., Reinecke, A., Freshour, G., Zabotina, O.A., Hahn, M.G., Burgert, I., Pauly, M., et al. (2008). Disrupting two Arabidopsis thaliana xylosyltransferase genes results in plants deficient in xyloglucan, a major primary cell wall component. Plant Cell 20:1519-1537.

Chiniquy, D., Varanasi, P., Oh, T., Harholt, J., Katnelson, J., Singh, S., Auer, M., Simmons, B., Adams, P.D., Scheller, H.V., et al. (2013). Three Novel Rice Genes Closely Related to the Arabidopsis IRX9, IRX9L, and IRX14 Genes and Their Roles in Xylan Biosynthesis. Front. Plant Sci. 4:83.

Doblin, M.S., Johnson, K.L., Humphries, J., Newbigin, E.J., and Bacic, A. (2014). Are designer plant cell walls a realistic aspiration or will the plasticity of the plant's metabolism win out? Curr Opin Biotechnol 26:108-114.

Doblin, M.S., Pettolino, F., and Bacic, A. (2010). Plant cell walls: the skeleton of the plant world. Functional Plant Biology 37:357-381.

Du, Q., Pan, W., Tian, J., Li, B., and Zhang, D. (2013). The UDP-glucuronate decarboxylase gene family in Populus: structure, expression, and association genetics. PloS one 8:e60880.

Earley, K.W., Haag, J.R., Pontes, O., Opper, K., Juehne, T., Song, K., and Pikaard, C.S. (2006). Gateway-compatible vectors for plant functional genomics and proteomics. Plant J. 45:616-629.

Ebert, B., Rautengarten, C., Guo, X., Xiong, G., Stonebloom, S., Smith-Moritz, A.M., Herter, T., Chan, L.J., Adams, P.D., Petzold, C.J., et al. (2015). Identification and Characterization of a Golgi-Localized UDP-Xylose Transporter Family from Arabidopsis. Plant Cell 27:1218-1227.

Edgar, R.C. (2004). MUSCLE: a multiple sequence alignment method with reduced time and space complexity. BMC Bioinformatics 5:113.

Egelund, J., Damager, I., Faber, K., Olsen, C.E., Ulvskov, P., and Petersen, B.L. (2008). Functional characterisation of a putative rhamnogalacturonan II specific xylosyltransferase. FEBS Lett. 582:3217-3222.

Egelund, J., Petersen, B.L., Motawia, M.S., Damager, I., Faik, A., Olsen, C.E., Ishii, T., Clausen, H., Ulvskov, P., and Geshi, N. (2006). Arabidopsis thaliana RGXT1 and RGXT2 encode Golgi-localized (1,3)-alpha-D-xylosyltransferases involved in the synthesis of pectic rhamnogalacturonan-II. The Plant cell 18:2593-2607.

Gotting, C., Kuhn, J., Zahn, R., Brinkmann, T., and Kleesiek, K. (2000). Molecular cloning and expression of human UDP-d-Xylose:proteoglycan core protein beta-d-xylosyltransferase and its first isoform XT-II. J. Mol. Biol. 304:517-528.

Harper, A.D., and Bar-Peled, M. (2002). Biosynthesis of UDP-xylose. Cloning and characterization of a novel Arabidopsis gene family, UXS, encoding soluble and putative membrane-bound UDP-glucuronic acid decarboxylase isoforms. Plant Physiol. 130:2188-2198.

Hayashi, T., Koyama, T., and Matsuda, K. (1988). Formation of UDP-Xylose and Xyloglucan in Soybean Golgi Membranes. Plant Physiol. 87:341-345.

Jensen, J.K., Johnson, N.R., and Wilkerson, C.G. (2014). Arabidopsis thaliana IRX10 and two related proteins from psyllium and Physcomitrella patens are xylan xylosyltransferases. Plant J. 80:207-215.

Jensen, J.K., Sorensen, S.O., Harholt, J., Geshi, N., Sakuragi, Y., Moller, I., Zandleven, J., Bernal, A.J., Jensen, N.B., Sorensen, C., et al. (2008). Identification of a xylogalacturonan xylosyltransferase involved in pectin biosynthesis in Arabidopsis. The Plant cell 20:1289-1302.

Keppler, B.D., and Showalter, A.M. (2010). IRX14 and IRX14-LIKE, two glycosyl transferases involved in glucuronoxylan biosynthesis and drought tolerance in Arabidopsis. Mol. Plant 3:834-841.

Kobayashi, M., Nakagawa, H., Suda, I., Miyagawa, I., and Matoh, T. (2002). Purification and cDNA cloning of UDP-D-glucuronate carboxy-lyase (UDP-D-xylose synthase) from pea seedlings. Plant & cell physiology 43:1259-1265.

Krogh, A., Larsson, B., von Heijne, G., and Sonnhammer, E.L.L. (2001). Predicting transmembrane protein topology with a hidden Markov model: Application to complete genomes. J. Mol. Biol. 305:567-580.

Lee, C., O'Neill, M.A., Tsumuraya, Y., Darvill, A.G., and Ye, Z.H. (2007). The irregular xylem9 mutant is deficient in xylan xylosyltransferase activity. Plant Cell Physiol. 48:1624-1634.

Lee, C., Teng, Q., Huang, W., Zhong, R., and Ye, Z.H. (2010). The Arabidopsis family GT43 glycosyltransferases form two functionally nonredundant groups essential for the elongation of glucuronoxylan backbone. Plant Physiol. 153:526-541.

Lee, C., Zhong, R., and Ye, Z.H. (2012). Arabidopsis family GT43 members are xylan xylosyltransferases required for the elongation of the xylan backbone. Plant Cell Physiol. 53:135-143.

Liu, X.L., Liu, L., Niu, Q.K., Xia, C., Yang, K.Z., Li, R., Chen, L.Q., Zhang, X.Q., Zhou, Y., and Ye, D. (2011). Male gametophyte defective 4 encodes a rhamnogalacturonan II xylosyltransferase and is important for growth of pollen tubes and roots in Arabidopsis. Plant J. 65:647-660.

McCartney, L., Marcus, S.E., and Knox, J.P. (2005). Monoclonal antibodies to plant cell wall xylans and arabinoxylans. J Histochem Cytochem 53:543-546.

Molhoj, M., Verma, R., and Reiter, W.D. (2003). The biosynthesis of the branched-chain sugar d-apiose in plants: functional cloning and characterization of a UDP-d-apiose/UDP-d-xylose synthase from Arabidopsis. Plant J. 35:693-703.

Nelson, B.K., Cai, X., and Nebenfuhr, A. (2007). A multicolored set of in vivo organelle markers for co-localization studies in Arabidopsis and other plants. Plant J. 51:1126-1136.

Øbro, J., Harholt, J., Scheller, H.V., and Orfila, C. (2004). Rhamnogalacturonan I in Solanum tuberosum tubers contains complex arabinogalactan structures. Phytochemistry 65:1429-1438.

Okazawa, K., Sato, Y., Nakagawa, T., Asada, K., Kato, I., Tomita, E., and Nishitani, K. (1993). Molecular cloning and cDNA sequencing of endoxyloglucan transferase, a novel class of glycosyltransferase that mediates molecular grafting

751 between matrix polysaccharides in plant cell walls. J. Biol. Chem. 268:25364-25368.
752 Pattathil, S., Harper, A.D., and Bar-Peled, M. (2005). Biosynthesis of UDP-xylose: characterization of membrane-bound
753 AtUxs2. Planta 221:538-548.
754 Pauly, M., and Keegstra, K. (2010). Plant cell wall polymers as precursors for biofuels. Current opinion in plant biology
755 13:305-312.
756 Peña, M.J., Zhong, R., Zhou, G.K., Richardson, E.A., O'Neill, M.A., Darvill, A.G., York, W.S., and Ye, Z.H. (2007). Arabidopsis
757 irregular xylem8 and irregular xylem9: implications for the complexity of glucuronoxylan biosynthesis. Plant
758 Cell 19:549-563.
759 Petersen, P.D., Lau, J., Ebert, B., Yang, F., Verhertbruggen, Y., Kim, J.S., Varanasi, P., Suttangkakul, A., Auer, M., Loque, D.,
760 et al. (2012). Engineering of plants with improved properties as biofuels feedstocks by vessel-specific
761 complementation of xylan biosynthesis mutants. Biotechnology for biofuels 5.
762 Pettolino, F.A., Walsh, C., Fincher, G.B., and Bacic, A. (2012). Determining the polysaccharide composition of plant cell
763 walls. Nat. Protoc. 7:1590-1607.
764 Ray, P.M. (1980). Cooperative action of beta-glucan synthetase and UDP-xylose xylosyl transferase of Golgi membranes
765 in the synthesis of xyloglucan-like polysaccharide. Biochim. Biophys. Acta 629:431-444.
766 Reiter, W.D. (2008). Biochemical genetics of nucleotide sugar interconversion reactions. Curr. Opin. Plant Biol.
767 11:236-243.
768 Reiter, W.D., and Vanzin, G.F. (2001). Molecular genetics of nucleotide sugar interconversion pathways in plants. Plant
769 Mol. Biol. 47:95-113.
770 Rodgers, M.W., and Bolwell, G.P. (1992). Partial purification of Golgi-bound arabinosyltransferase and two isoforms of
771 xylosyltransferase from French bean (Phaseolus vulgaris L.). Biochem. J. 288 (Pt 3):817-822.
772 Rosenberger, A.F., Hangelmann, L., Hofinger, A., and Wilson, I.B. (2012). UDP-xylose and UDP-galactose synthesis in
773 Trichomonas vaginalis. Molecular and biochemical parasitology 181:53-56.
774 Schmittgen, T.D., and Livak, K.J. (2008). Analyzing real-time PCR data by the comparative C(T) method. Nat. Protoc.
775 3:1101-1108.
776 Seifert, G.J. (2004). Nucleotide sugar interconversions and cell wall biosynthesis: how to bring the inside to the outside.
777 Curr. Opin. Plant Biol. 7:277-284.
778 Sparkes, I.A., Runions, J., Kearns, A., and Hawes, C. (2006). Rapid, transient expression of fluorescent fusion proteins in
779 tobacco plants and generation of stably transformed plants. Nat. Protoc. 1:2019-2025.
780 Stevenson, T.T., McNeil, M., Darvill, A.G., and Albersheim, P. (1986). Structure of Plant Cell Walls : XVIII. An Analysis of
781 the Extracellular Polysaccharides of Suspension-Cultured Sycamore Cells. Plant Physiol. 80:1012-1019.
782 Strasser, R., Mucha, J., Mach, L., Altmann, F., Wilson, I.B., Glossl, J., and Steinkellner, H. (2000). Molecular cloning and
783 functional expression of beta1, 2-xylosyltransferase cDNA from Arabidopsis thaliana. FEBS Lett. 472:105-108.
784 Suzuki, K., Suzuki, Y., and Kitamura, S. (2003). Cloning and expression of a UDP-glucuronic acid decarboxylase gene in
785 rice. Journal of experimental botany 54:1997-1999.
786 Suzuki, K., Watanabe, K., Masumura, T., and Kitamura, S. (2004). Characterization of soluble and putative
787 membrane-bound UDP-glucuronic acid decarboxylase (OsUXS) isoforms in rice. Arch. Biochem. Biophys.
788 431:169-177.
789 Tamura, K., Shimada, T., Kondo, M., Nishimura, M., and Hara-Nishimura, I. (2005). KATAMARI1/MURUS3 Is a novel golgi
790 membrane protein that is required for endomembrane organization in Arabidopsis. The Plant cell
791 17:1764-1776.
792 UniProt Consortium. (2015). UniProt: a hub for protein information. Nucleic Acids Res. 43:D204-D212.
793 Urbanowicz, B.R., Pena, M.J., Moniz, H.A., Moremen, K.W., and York, W.S. (2014). Two Arabidopsis proteins synthesize
794 acetylated xylan in vitro. Plant J. 80:197-206.

795 Urbanowicz, B.R., Pena, M.J., Ratnaparkhe, S., Avci, U., Backe, J., Steet, H.F., Foston, M., Li, H., O'Neill, M.A., Ragauskas,
796 A.J., et al. (2012). 4-O-methylation of glucuronic acid in Arabidopsis glucuronoxylan is catalyzed by a domain of
797 unknown function family 579 protein. Proceedings of the National Academy of Sciences of the United States of
798 America 109:14253-14258.
799 Wierenga, R.K., Terpstra, P., and Hol, W.G. (1986). Prediction of the occurrence of the ADP-binding beta alpha beta-fold
800 in proteins, using an amino acid sequence fingerprint. Journal of molecular biology 187:101-107.
801 Winter, D., Vinegar, B., Nahal, H., Ammar, R., Wilson, G.V., and Provart, N.J. (2007). An "Electronic Fluorescent
802 Pictograph" browser for exploring and analyzing large-scale biological data sets. PLOS ONE 2:e718.
803 Wu, A.M., Hornblad, E., Voxeur, A., Gerber, L., Rihouey, C., Lerouge, P., and Marchant, A. (2010). Analysis of the
804 Arabidopsis IRX9/IRX9-L and IRX14/IRX14-L pairs of glycosyltransferase genes reveals critical contributions to
805 biosynthesis of the hemicellulose glucuronoxylan. Plant Physiol. 153:542-554.
806 Wu, A.M., Rihouey, C., Seveno, M., Hornblad, E., Singh, S.K., Matsunaga, T., Ishii, T., Lerouge, P., and Marchant, A. (2009).
807 The Arabidopsis IRX10 and IRX10-LIKE glycosyltransferases are critical for glucuronoxylan biosynthesis during
808 secondary cell wall formation. Plant J. 57:718-731.
809 Yu, Q., Zhuang, X., Yuan, Z., Wang, Q., Qi, W., Wang, W., Zhang, Y., Xu, J., and Xu, H. (2010). Two-step liquid hot water
810 pretreatment of Eucalyptus grandis to enhance sugar recovery and enzymatic digestibility of cellulose.
811 Bioresour. Technol. 101:4895-4899.
812 Zabotina, O.A., van de Ven, W.T., Freshour, G., Drakakaki, G., Cavalier, D., Mouille, G., Hahn, M.G., Keegstra, K., and
813 Raikhel, N.V. (2008). Arabidopsis XXT5 gene encodes a putative alpha-1,6-xylosyltransferase that is involved in
814 xyloglucan biosynthesis. Plant J. 56:101-115.
815 Zhang, Q., Shirley, N., Lahnstein, J., and Fincher, G.B. (2005). Characterization and expression patterns of
816 UDP-D-glucuronate decarboxylase genes in barley. Plant Physiol. 138:131-141.
817 Zhao, X., Ouyang, K., Gan, S., Zeng, W., Song, L., Zhao, S., Li, J., Doblin, M.S., Bacic, A., Chen, X.Y., et al. (2014).
818 Biochemical and molecular changes associated with heteroxylan biosynthesis in Neolamarckia cadamba
819 (Rubiaceae) during xylogenesis. Front. Plant Sci. 5:602.
820 Zhong, R., Pena, M.J., Zhou, G.K., Nairn, C.J., Wood-Jones, A., Richardson, E.A., Morrison, W.H., 3rd, Darvill, A.G., York,
821 W.S., and Ye, Z.H. (2005). Arabidopsis fragile fiber8, which encodes a putative glucuronyltransferase, is essential
822 for normal secondary wall synthesis. The Plant cell 17:3390-3408.
823 Zhong, R., Teng, Q., Lee, C., and Ye, Z.H. (2014). Identification of a disaccharide side chain
824 2-O-alpha-D-galactopyranosyl-alpha-D-glucuronic acid in Arabidopsis xylan. Plant signaling & behavior
825 9:e27933.
826
827
828

829 **Table 1.** Monosaccharide composition (mol %) of AIR from cell wall extracts of stem material from
830 6-week old plants. The data represent means ± SE (n = 3).
831

	WT (Col-0)	*uxs1uxs2uxs4*	*uxs3uxs5uxs6*
Fucose	0.97±0.00	0.62±0.01	0.79±0.03
Rhamnose	4.05±0.02	4.07±0.03	5.93±0.21
Arabinose	3.83±0.03	3.45±0.02	7.86±0.26
Galactose	9.84±0.05	9.51±0.10	12.67±0.30
Glucose	20.48±0.03	19.12±0.11	21.89±0.64
Xylose	55.8±0.05	58.34±0.20	44.21±0.48
GalA	4.45±0.11	4.18±0.06	6.32±0.31
GlcA	0.57±0.04	0.70±0.06	0.33±0.05

832
833

834

835 **Table 2.** The number-average molecular weight (M_n) and weight-average molecular weight (M_w) of
836 the non-cellulosic polysaccharides extracted with 1N KOH and 2N KOH from wild type (H1),
837 *uxs1uxs2uxs4* (H2) and *uxs3uxs5uxs6* (H3) fraction.

838

	1N KOH			2N KOH		
g/mol	H_1	H_2	H_3	H_1	H_2	H_3
M_w	90180	64390	24270	107600	73010	38460
M_n	22740	9795	9722	10750	9102	10020
M_w/M_n	3.97	6.57	2.50	10.01	8.02	3.84

839

840

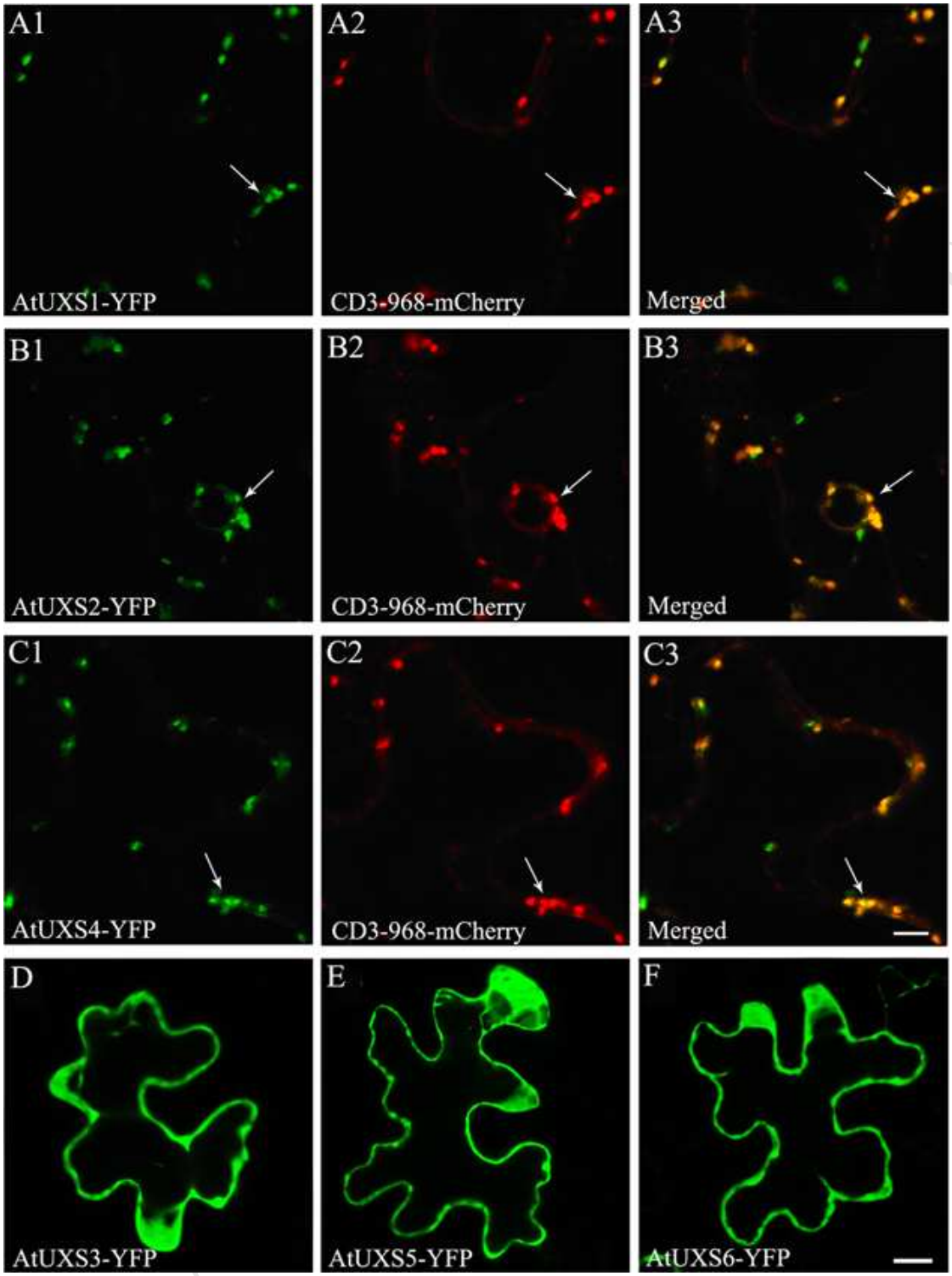

Figure 1. Subcellular localization of AtUXS proteins. C-terminal YFP fusions with individual *AtUXS* genes were expressed in *N. benthamiana*. UXS1-YFP, UXS2-YFP, and UXS4-YFP images are shown in (A1), (B1) and (C1), respectively. Golgi-localized CD3-968-mCherry images are shown in (A2), (B2) and (C2), and the merged images are shown in (A3), (B3) and (C3), respectively. Confocal images from (D) to (F) show AtUXS3-YFP, AtUXS5-YFP and AtUXS6-YFP, respectively. Bar = 5 μm for (A1) to (C3), Bar = 10μm for (D) to (F).

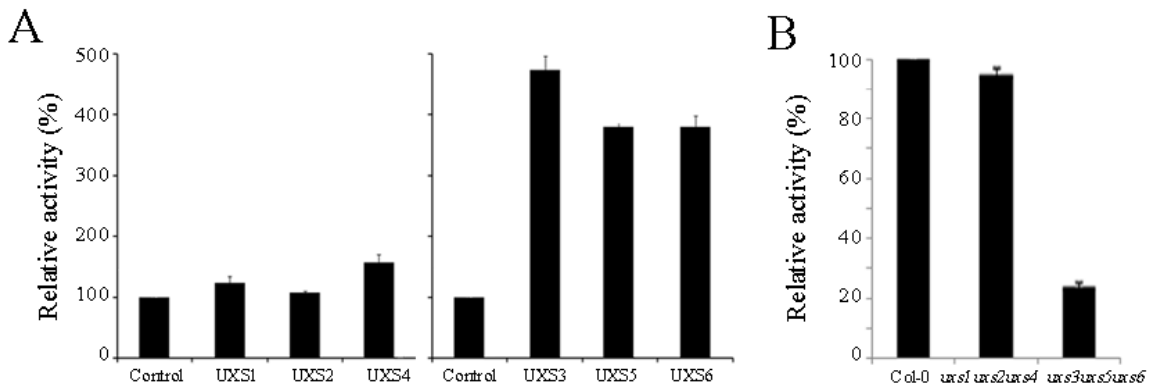

Figure 2. The activities of AtUXS1-6 heterologously expressed in *N. benthamiana*. Total tobacco proteins were extracted from 3 d-old inoculated tobacco leaves and their UXS activity for conversion of UDP-GlcA to UDP-Xyl measured. (A) Heterologously expressed UXS activity was measured by the conversion rate of UDP-GlcA to UDP-Xyl and the control injected with empty vector was set as 100%. (B) The relative activities of UXS in wild type and mutant *uxs1uxs2uxs4* (Group II) and *uxs3uxs5uxs6* (Group I) extracts was determined. Total protein was extracted from 2-week-old plants growing in MS medium. The average of three biological replicates +/- standard error are shown.

858

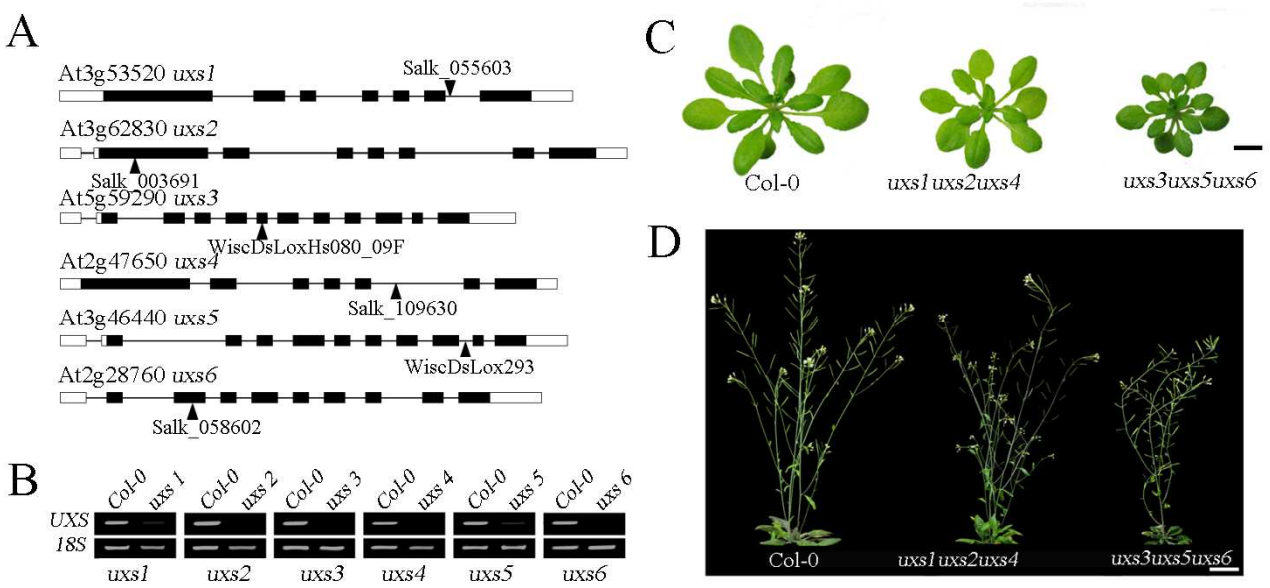

859

860 Figure 3. T-DNA insertion lines for the six Arabidopsis *UXS* genes and mutant plant phenotypes. (A)
861 Intron-exon structure of *UXS* genes and location of T-DNA insertion in mutant alleles (triangles).
862 Boxes represent exons and lines introns. *uxs1*, *uxs2*, *uxs3*, *uxs4*, *uxs5* and *uxs6* have a T-DNA
863 insertion in At3g53520, At3g62830, At5g59290, At2g47650, At3g46440 and At2g28760 loci,
864 respectively. (B) RT-PCR analysis reveals no transcript in lines of *uxs2*, *uxs3*, *uxs4* and *uxs6* mutants
865 and reduced transcript in *uxs1* and *uxs5* compared to wild type (Col-0). 18S ribosomal PCR results
866 were used as the loading control. A total of three biological replicates were analysed for each line.
867 The primers used for RT-PCR are outlined in Supplemental Table 4. (C) 5-week-old rosette leaves of
868 WT Col-0 and the triple mutants *uxs1uxs2uxs4* and *uxs3uxs5uxs6*. Bar = 1cm. (D) 8-week-old plants
869 of WT Col-0 and the triple mutants, *uxs1uxs2uxs4* and *uxs3uxs5uxs6*. Bar = 2cm.

870

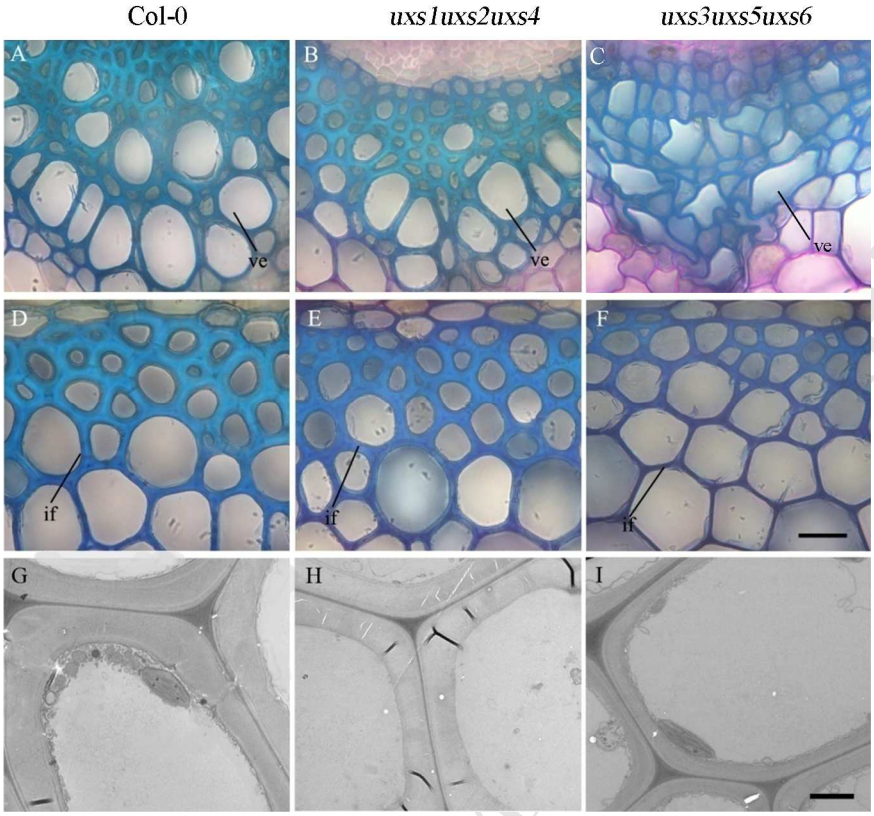

Figure 4. Vessel morphology and thickness of secondary cell walls of WT (Col-0) and triple mutants, *uxs1uxs2uxs4* and *uxs3uxs5uxs6*. (A) to (C) Transverse sections of stems of WT (Col-0) and the triple mutants, *uxs1uxs2uxs4* and *uxs3uxs5uxs6*. Misshapen vessels in *uxs3uxs5uxs6* are apparent. (D) to (F) Transverse sections of WT (Col-0) and the triple mutants, *uxs1uxs2uxs4* and *uxs3uxs5uxs6* from the interfascicular fiber region showing reduced thickness in *uxs3uxs5uxs6*. (G) to (I) Transmission electron micrographs of WT (Col-0) and the triple mutants, *uxs1uxs2uxs4* and *uxs3uxs5uxs6* in the interfascicular fiber region. Bar = 10 μm in (A-F); Bar = 3 μm in (G-I). ve, vessel; if, interfascicular fibers.

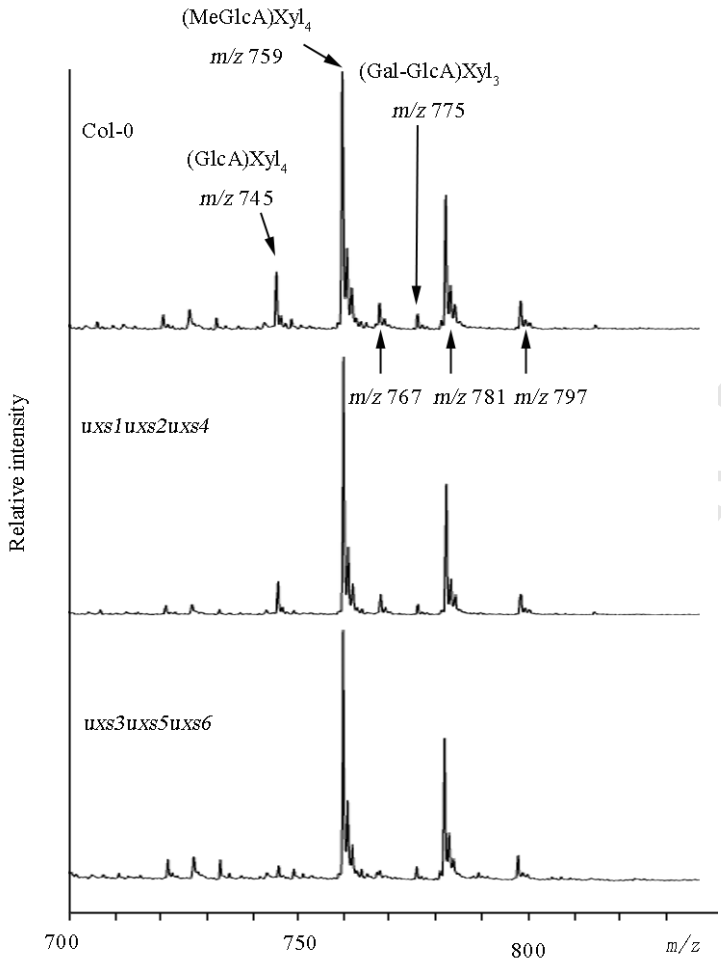

Figure 5. MALDI-TOF mass spectrum of xylo-oligomers from wild type and *uxs1uxs2uxs4* and *uxs3uxs5uxs6* triple mutants. The KOH extracted fraction from AIR of stem material was digested with an endo-xylanase and the resultant oligosaccharides analysed by MALDI-TOF MS. The identity of prominent pseudo-molecular ion peaks (*m/z*) 745, 759, 767, 781 and 797 are attributed to (GlcA)Xyl_4-Na^+, (MeGlcA)Xyl_4-Na^+, (Gal-GlcA)Xyl_3-Na^+, (GlcA)Xyl_4-$2Na^+$, (MeGlcA)Xyl_4-$2Na^+$ and (Gal-GlcA)Xyl_3-$2Na^+$, respectively.

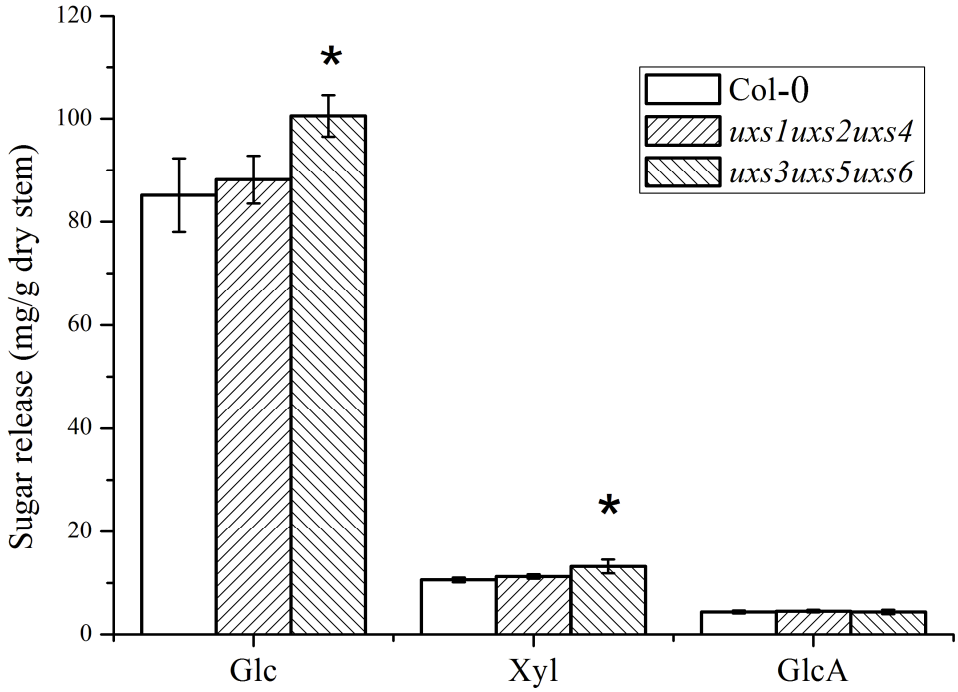

Figure 6. Saccharification analyses. Increased digestibility was observed in *uxs1uxs2uxs4* and *uxs3uxs5uxs6* triple mutant plants compared to wild type. Values show average ± SE (n = 5). * indicates a significant difference from the wild type (t-test, $p < 0.01$).

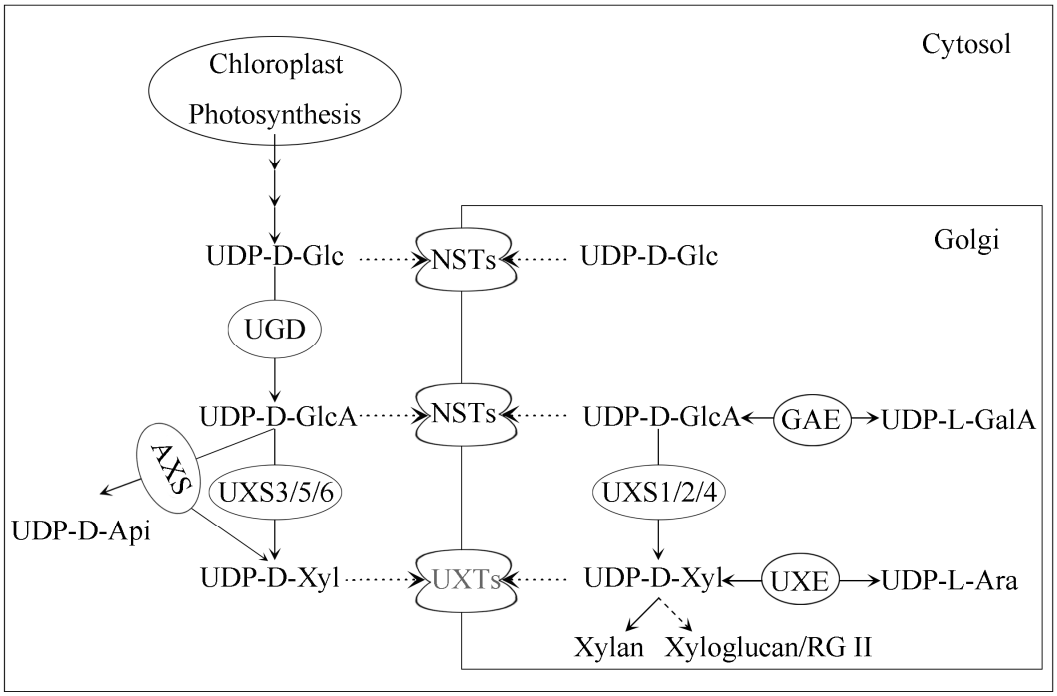

Figure 7. Overview of metabolic pathways and the compartmentalization of nucleotide sugar interconverting enzymes that are involved in UDP-D-Xyl synthesis between the cytosol and Golgi lumen. UGD: UDP-D-Glc dehydrogenase. GAE: UDP-GlcA epimerase. AXS: UDP-D-Api/UDP-D-Xyl synthase. UXE: UDP-D-Xyl 4-epimerase. UXS: UDP-glucuronic acid decarboxylase. NSTs: nucleotide sugar transporters, and UXTs: UDP-Xyl transporters.